The DOI for this manuscript is doi: 10.1175/JCLI-D-12-00697.1

The final published version of this manuscript will replace the preliminary version at the above DOI once it is available.

If you would like to cite this EOR in a separate work, please use the following full citation:

Grassi, B., G. Redaelli, and G. Visconti, 2013: Arctic sea-ice reduction and extreme climate events over the Mediterranean region. J. Climate. doi:10.1175/JCLI-D-12-00697.1, in press.

Arctic sea-ice reduction and extreme climate events over the Mediterranean region

Barbara Grassi, Gianluca Redaelli and Guido Visconti

University of L'Aquila, CETEMPS/Department of Physical and Chemical Sciences, Coppito-L'Aquila, Italy

Corresponding author: Barbara Grassi (e-mail:barbara.grassi@aquila.infn.it)

Abstract.

During the last decade, Arctic sea-ice cover has experienced an accelerated decline that has been suggested to drive the increased occurrence of extremely cold winter events over continental Europe. Observations and modeling studies seem to support the idea that Mediterranean climate is also changing. In this work we estimate potential effects on the Mediterranean basin, during the winter period, of Arctic sea-ice reduction. Two sets of simulations have been performed by prescribing different values of sea-ice concentrations (50% and 20%) on the Barents-Kara (BK) seas in the CAM3/NCAR atmospheric GCM, as representative of idealized sea-ice present and future conditions. Global model simulations have then been used to run RegCM4/ICTP regional model over central Europe and the Mediterranean domain. Simulations evidence a large scale atmospheric circulation response to sea ice reduction, resembling the negative phase of the Arctic Oscillation (AO) and characterized by a wave activity flux from the North Atlantic toward the Mediterranean basin, during winter months. We find an increase in the occurrence and intensity of extreme cold events, over continental Europe, and extreme precipitation events, over all the Mediterranean basin. In particular, simulations suggest an increased risk of winter flooding on southern Italy, Greece and Iberian peninsula.

1. Introduction

Observations and modeling studies seem to support the idea that Mediterranean climate is changing. In particular, the possibility that the climate in this region could become more variable and extreme is currently under investigation. An increased frequency of extreme event occurrence has been registered during latest years (e.g.: European summer heat wave in 2003; 2004 winter cold wave in Turkey; heavy snow in Balkan in 2005 and in Italy in 2012). Both observational (Alexander et al. 2006; Klein Tank and Konnen 2003) and modeling studies (Meehl et al. 2004; Kharin et al. 2007; Kodra et al. 2011) suggest that while global mean temperature will significantly increase by the end of the 21st century, extreme cold events will not disappear.

During last decades, pronounced warming was observed in the Arctic during winter. This warming was accompanied by a rapid decrease in sea-ice cover that is particularly pronounced in the Barents Sea (Stroeve et al. 2007). The Arctic winter sea-ice retreat has been related to an increase of the Atlantic inflow to the western Barents sea and the increased delivery of oceanic heat to the ice-sheet margin (Stroeve et al. 2011; Joughin et al. 2012; Arthun et al. 2012). Future scenarios also indicate abrupt reduction of Arctic summer sea-ice related to increasing ocean heat transport to the Arctic (Holland et al. 2006).

Some dynamical mechanisms have been suggested to explain sea-ice variability influence on the atmospheric circulation. These include the formation of stationary Rossby wave trains and the forcing of the North Atlantic Oscillation toward a negative phase (see e.g. Yamamoto et al. 2006; Honda et al. 2009). An involvement of change in cyclone paths, also explaining the persistence during winter of the response to anomalous ice cover during autumn, has been recently suggested by Inoue et al. (2012). The authors, by using NCEP-NCAR reanalysis, showed that during light ice years the lower baroclinicity over the Barents Sea prevents cyclones from traveling eastward. They also used a composite analysis of heavy and light ice years of all cyclone events to show that during light ice years an anticyclonic anomaly prevailed along the Siberian coast of the Barents Sea leading to anomalous warm advection over the Barents Sea and cold advection over eastern Siberia.

Honda et al. (2009) and Petoukhov and Semenov (2010) showed that the anomalous decrease of wintertime Arctic sea-ice concentration could increase the probability of cold winter extremes over large areas, including continental Europe. Also Liu et al. 2102, found that the recent decline of Arctic sea-ice has played a critical role in recent cold winters over large part of northern continents.

On the light of the above mentioned studies, in the present work we focus our interest on the possibility that dynamical perturbations driven by Arctic sea ice decrease could also impact the Mediterranean area, in particular changing the intensity and the probability of extreme climate events.

An increasing trend in the occurrence of extreme winter precipitation events (from heavy to torrential) in Spain and Italy has been identified by Toreti et al. (2010). Between January 1950 and October 2009, 395 severe flood and storm events were also reported by EM-DAT (2009) for 19 Mediterranean countries. During autumn 2011, severe flood events hit Liguria, Tuscany and Sicily regions, in Italy.

General Circulation Models (GCMs) are useful tools to study future climate change, but their application to regional climatic process studies is limited due to the coarse spatial resolution (approximately 2.5° in latitude–longitude). A common problem with global climate models is the fact that their grids do not always resolve important topographic features which determine the spatial variability of rainfall at regional scales (Smith et al. 2013). Regional modeling studies have shown that an increase in resolution generally leads to a better simulation of the precipitation statistics, including extremes (e.g. Huntingford et al. 2003). Fine-scale processes have been identified to play a critical role in the response of extreme precipitation events (Diffenbaugh et al. 2005). For these reasons, global GCMs, while representing the best tool to make future climate scenario projections, do to their coarse spatial resolution usually require a downscaling procedure for regional impact-oriented studies. Brankovic et al. (2012) assessed a good ability of RegCM to reproduce the spatial distribution of extreme temperatures and precipitations over Croatia by comparing results from a “present-day” simulation driven by the ECHAM5/MPI-OM global climate model simulation for 30 years during the 20th century (1961-1990) with Croatian station data. They also highlighted the need for using high resolution regional model to accurately reproduce climate extremes which are often related to sharp orographic gradients or to complex small-scale orography.

Both Gao et al. (2006), by using a high-resolution regional climate model, and Goubanova and Li (2007), by using a variable-grid general circulation model, evaluated changes in precipitation around the Mediterranean basin, under the IPCC SRES-A2 emission scenario. In particular, during winter, they suggested that this region will experience a decrease of total precipitation but more intense precipitation events.

In this work we estimate the potential effects on the Mediterranean basin of Arctic sea-ice reduction during the winter period. To this end, global dynamical fields from an atmospheric GCM are used to initialize and force a regional climate model at higher horizontal resolution.

Section 2 describes the used models and the performed simulations. Also, a description of the indexes used to identify extreme events is provided. Results are examined in Section 3 while conclusions are summarized in Section 4.

2. Models and Simulations

Two idealized simulation cases have been performed with NCAR/CAM3 GCM (Collins et al. 2006). The model has been used at a T42 resolution (about 2.8° x 2.8°) with 26 vertical layers in a hybrid-sigma coordinate system, ranging from the surface to 2.917 hPa. Ozone, Sea Surface Temperature (SST) and sea-ice climatological boundary conditions have been taken from the standard datasets provided with the model. At sea level, CAM3 at a T42 resolution reproduces the basic observed patterns of the pressure field. However, the model is known to have a bias at high latitudes characterized by simulated pressures that are too low poleward of 50° latitude in both the Northern and Southern hemispheres. In particular, during winter, the Iceland low is too deep and it extends too far over Eurasia and the Arctic Basin (Hurrell et al. 2006).

Following the approach used in previous studies (Grassi et al. 2008; Grassi et al. 2012), i.e. considering a repeating annual cycle of the boundary conditions, we run the model for 12 consecutive years, producing 12 yearly realizations that have been used to generate a statistical base for analysis. More in detail, CAM3 simulations have been forced by prescribing analyzed climatological monthly mean values of SST, provided with the model and obtained by merging HadlSST (Rayner et al. 2003) with the NOAA's OI.v2 SST (Reynolds et al. 2002). The climatological value is obtained by averaging data for the 1950-2001 time period. Sea-ice concentration has been also globally set to the climatological value, with the only exception of the Barents-Kara (BK) region where, from November to April, sea-ice concentration has been set to 50% and 20% values to respectively produce the two simulation cases hereafter referred as 50%ICE and 20%ICE. Based on Kern et al. 2010, these two concentration values have been chosen as representative of present (50% sea-ice concentration) and future (20% sea-ice concentration) winter conditions during next decades. Sea-ice concentration fields for the two simulation cases are shown in Fig. 1. The prescribed idealized sea-ice concentrations are consistent with present day ice cover (1980-2000 time period) and projected ice cover (2080-2100 time period) for the SRES A1B scenario, during winter (IPCC 2007; http://www.ipcc.ch/publications_and_data/ar4/wg1/en/figure-10-14.html).

Results from CAM3 simulations have then been used to force a regional climate model during the winter period, i.e. from January to March. The three-dimensional mesoscale model used in this study is RegCM4/ICTP (Giorgi et al. 2012). The chosen model domain covers the Mediterranean region and surrounding areas, from Spain to Turkey and from Northern Africa to the Baltic sea. The model is run with a horizontal grid spacing of about 60 km and the standard vertical configuration with 18 sigma layers. To obtain a larger ensemble of initial/boundary conditions for RegCM4, each set of u, v and T field simulated by CAM3 has been perturbed by adding/subtracting to each variable a random quantity equal to 0 to .5 times the standard deviation of its weekly distribution. This process has been repeated three times obtaining a total ensemble of 48 (3*12 perturbed + 12 unperturbed fields) sets of initial/boundary conditions for RegCM4 for each simulated case (50%ICE and 20%ICE). The lateral boundary conditions are provided from CAM3 to RegCM4 through the selection of a lateral buffer zone and the use of a nudging procedure that interpolates the driving large scale fields onto the model grid then applying a relaxation/diffusion term (Giorgi et al. 1993). Topography of RegCM4 is provided at a resolution of approximately 1 km.

Cold temperature and heavy precipitation events have been analyzed on a grid-point basis (see e.g. Bell et al. 2004). From the distributions of daily minimum and maximum near surface temperature (T_{min}, T_{max}) and total daily precipitation (P_{tot}) values, the 5-th (T_{min}^{05} / P_{tot}^{05}) and 95-th (T_{max}^{95} / P_{tot}^{95}) percentile have been calculated at each grid-point and for each of the 48 simulated winters to identify, respectively, extreme cold / drought and hot /

rainy events. The mean change in the number of extreme cold (hot) daily events has been calculated as the change in the total number of days per winter in which the daily minimum (maximum) temperature fell below (above) $T_{min}{}^{05}{}_{(50\%)}$ ($T_{max}{}^{95}{}_{(50\%)}$), where the “50%” subscript means that the percentile is calculated for the 50%ICE case that is assumed as background reference condition. In a similar way, the indexes that characterize extreme drought (rainy) events, has been defined by considering the 5th (95th) percentile of the seasonal daily precipitation distribution, $P_{tot}{}^{05}$ ($P_{tot}{}^{95}$). This percentile value has been then used to calculate the change in the number of extreme precipitation events per winter, corresponding to the change in the number of days in which the mean precipitation value fell below (above) $P_{tot}{}^{05}{}_{(50\%)}$ ($P_{tot}{}^{95}{}_{(50\%)}$).

3.Results

The response to the prescribed idealized sea-ice reduction is investigated in terms of difference in means between 20%ICE and 50%ICE simulated cases. The means are, respectively, 12 or 48 winter averages, for CAM3 or RegCM4. The significance of the difference in means is assessed using a Student’s t test.

The dynamical response to sea-ice reduction has been preliminarily studied on the large-scale by examining CAM3 simulation results. The analysis of mean changes of sea level pressure (SLP) shows the development during January of a statistically significant signal (Fig. 2, left). SLP shows an anticyclonic anomaly near the Taymyr Peninsula that strongly resembles the SLP anomaly pattern found by Inoue et al. (2012) in their composite analysis, performed on NCEP-NCAR reanalysis data, between light and heavy ice years. In the study by Inoue et al., the SLP signal has been attributed to a change of the cyclone tracks due to the lower baroclinicity over the Barents Sea during the light ice years which prevented cyclones from traveling eastward. To this end, an algorithm for cyclone identification and tracking has been used. Even if a complete study of the cyclone tracks is beyond the scope of the present paper, the analysis of the change in the baroclinicity between 20%ICE and 50%ICE simulation cases seems to support the hypothesis that a mechanism similar to that discussed by Inoue et al. could also be active in our model. Figure 2 also shows the difference in the baroclinicity, which we calculate as the vertical zonal wind shear between 500 and 925 hPa, due to the introduction in November of the prescribed sea-ice perturbation. The statistically significant negative signal over the Scandinavian peninsula indicates a reduction of the baroclinicity simulated in the 20%ICE compared to the 50%ICE background case. Even if a different origin of the anticyclonic pattern cannot be definitively ruled out (i.e. it could follow from a difference in the model bias in the two simulated cases), the characteristics of the baroclinicity reduction in November are however consistent with a decrease in the number of cyclones reaching the Siberian coast during the following months. The signal on baroclinity disappears during the following months. These results are also consistent with previous studies (Deser et al. 2007; Deser et al. 2010; Jaiser et al. 2012) showing an initial early winter baroclinic response, followed then by a mid-winter barotropic response that reaches equilibrium 2-2.5 months after the initial sea-ice cover change and that resembles the North Atlantic Oscillation-Arctic Oscillation (NAO-AO) pattern. 500 hPa Gph response (Fig. 3, left) shows, during January, statistically significant positive anomalies over the Arctic region extending toward the North Atlantic sector and negative anomalies over the Balkan region with a minimum lower than -40 m. The pattern of 500 hPa Gph simulated for the 50%ICE background case is also shown for comparison purpose (Fig. 3, right). Results suggest that the response, which shows some resemblance to the pattern of the AO in its negative phase, leads to a weakening of the positive AO-like background structure. The 500 hPa Gph response seems to be related to the anticyclonic anomaly near the Taymyr Peninsula that leads to a clockwise circulation, then bringing anomalous cold air from northeastern Siberia toward central Europe and warm air toward the North Atlantic. The persistence of this warming can activate the wave flux toward the Mediterranean region which in turn creates the lower pressure anomaly. Figure 4 shows the response to the prescribed ice perturbation in terms of 250 hPa Gph, surface sensible and latent heat fluxes and 250 hPa wave activity flux (WAF), averaged during winter. Geopotential height wavelike anomalies suggest the occurrence of stationary Rossby waves excited by anomalous heat flux and associated with the propagation of WAF. The horizontal WAF (Takaya and Nakamura 2001) shows a strong wave propagation from the North Atlantic region southeastward into the lower latitudes reaching the Mediterranean basin. Honda et al. (2009) also found an eastward propagation of the horizontal WAF, impacting the Far East. T_{min} anomalies, calculated at the bottom level of CAM3 for January, February and March (Fig. 5), show positive values over the Arctic region and negative values over Eurasia, with a strong minimum over Asia, that progressively decreases from January to March, and a secondary minimum over continental Europe that is located over the Balkan peninsula during January and shifts toward the central and western Europe during February and March, with values up to -2°C. While the minimum over Eurasia is probably driven by the anticyclonic circulation over the eastern Arctic region, the minimum over Europe seems related to the intrusion of cold air from the North Atlantic into the Mediterranean basin due to WAF. This intrusion, which is a large scale dynamical effect and is prescribed in RegCM4 through the boundary conditions provided by CAM3, leads, when reaching the Mediterranean basin, to a heat flux from the sea. The higher grid resolution of RegCM4 produces differences, between global and regional model, in the simulation of the processes that involve orographic characteristics of the domain. The heat fluxes simulated by RegCM4 and CAM3 in the 50%ICE background case and in the response to the prescribed sea-ice reduction are shown in Fig. 6. The pattern of the heat fluxes are similar for the background case (Figs. 6 c,d), with maximum values on the eastern Mediterranean, and for the response to sea-ice reduction (Figs 6 a,b), with maximum values over the western Mediterranean region. However, CAM3 simulates an heat flux perturbation which is generally 50% higher than what found with RegCM4. This is probably related to the coarse resolution of CAM3, that seems unable to resolve the topography of the Italian peninsula.

The response to sea-ice reduction in terms of temperature extreme events appears to be correlated with the characteristics of the simulated heat fluxes. Figure 7a shows statistically significant negative anomalies of $\langle T_{min} \rangle$ (winter mean of T_{min} at 2 meters), extending over the European and Mediterranean regions with a minimum of about -1° over continental Europe. Over central Europe, and in particular over the Balkan peninsula, anomalies of T_{min}^{05} (Fig. 7b) are larger than anomalies in $\langle T_{min} \rangle$, with minimum values of about -3°C, suggesting a widening of the T_{min} distribution and a greater climate variability simulated in 20%ICE with respect to 50%ICE case. The large negative values of T_{min}^{05} over the Balkan peninsula indicate a strong intensification of extreme cold events in a region that matches the position of the secondary minimum of T_{min} perturbation during January (i.e. in a month usually characterized by the lowest winter temperatures), shown in Fig. 5a. Also, N_{cold} (corresponding to the mean number of days per winter characterized by a $T_{min} < T_{min}^{05}{}_{(50\%)}$, Fig. 7c) generally increases, up to 9 days over continental Europe, and up to 6 days over the Mediterranean basin and the Italian peninsula. The changes in $\langle T_{min} \rangle$, T_{min}^{05} and N_{cold} (Figs. 7 d,e,f) are fairly similar in CAM3 simulation, showing however a reduction of the area of the domain where the signal is statistically significant. This reduction reasonably follows from the stronger heat flux simulated by CAM3.

Changes of $\langle P_{tot} \rangle$ (winter mean P_{tot}), simulated by RegCM4 (Fig. 8a), show positive anomalies over the Mediterranean region and negative anomalies over continental Europe, generally lower than 2 mm/day. The response in P_{tot}^{95} (Fig. 8b) has a similar pattern but larger anomaly values, up to 5-6 mm/day. Maximum increases in the intensity of extreme precipitation events in the Mediterranean region are on southern Italy, Greece and Iberian peninsula. Also, maximum anomalies in the mean number of extreme precipitation events per winter, N_{rainy} (corresponding to the change of the number of days per winter characterized by a $P_{tot} > P_{tot}^{95}{}_{(50\%)}$), are simulated over southern Italy and Iberian peninsula (Fig. 8c), with values up to 9 days per winter. The pattern of precipitation change shows enhanced rainfall over the coastlines where there is an intensification of the onshore flow consistently with the cyclonic circulation response over the Mediterranean region (see Fig. 4), and reduced rainfall over continental Europe, probably related to a reduction of the westerly flow of moist air from the Atlantic. Changes of $<P_{tot}>$, P_{tot}^{95} and N_{rainy}, as simulated by CAM3, are shown in Figs. 8d,e,f. The comparison of Fig. 8a and 8d highlights a $<P_{tot}>$ intensification over coastlines, as simulated by RegCM4 with respect to CAM3. About P_{tot}^{95}, the strong intensification of extreme rainy events simulated by RegCM4 is not present in the response simulated by CAM3. The changes of P_{tot}^{95} simulated by CAM3 shows no dependency on the orography or coastlines and is characterized by values lower than 1 mm/day. The change of N_{rainy}, showing values up to 8-10 days both in RegCM4 and CAM3, indicates an increase in the frequency of extreme precipitation events. The difference in the characteristics of extreme precipitation events simulated by the two models highlights the importance of a more detailed orography in RegCM4, leading to convective processes activation and to an increase of precipitation events, even in presence of overall lower values of heat flux. RegCM4 simulations show, for the prescribed Arctic sea-ice reduction, a general greater risk of flooding over the southern Europe and in particular over coastline regions of the Mediterranean basin, highlighting an increase of both intensity and frequency of flood events.

Analyses performed on T_{max}^{95} / P_{tot}^{05}, not shown here, do not evidence a statistically significant increase in intensity or number of hot and drought extreme events in both CAM3 and RegCM4 simulations.

4. Conclusions

In this paper we estimated the potential climate response over the Mediterranean region to sea-ice concentration reduction (from 50% to 20%) on the BK seas, by using the RegCM4 regional climate model driven by large scale fields from CAM3 GCM. This response has been investigated in terms of changes in extremes of winter minimum temperature and total precipitation and in the number of extreme cold and rainy events, identified by examining high and low quantiles of the seasonal distributions.

Based on Arctic sea-ice trends (e.g. Kern et al. 2010) and IPCC projections (IPCC, 2007), the prescribed idealized sea-ice concentrations are reasonably representative of present and future (i.e. within the next decades) BK sea-ice conditions, and so we can look at the results as a possible future climatic scenario for the Mediterranean area.

Our main conclusions can be summarized as follows:

(1) results suggest a shift toward an overall more cold/rainy winter conditions on the Mediterranean basin and, in particular, a tendency toward an increased risk of flooding on southern Italy, Greece and Iberian peninsula. Also, temperature extreme events show an increase in intensity, over the Balkan peninsula, and in number, over continental Europe.

(2) The investigation of the dynamical perturbation leading to the remote response on the Mediterranean basin suggests the activation of a large scale mechanism consistent with those discussed in previous works. The response, following an initial baroclinic stage of adjustment, becomes progressively more barotropic and is characterized by a wave activity flux from the North Atlantic toward the Mediterranean basin and by a negative AO-like

pattern.

(3) When comparing global to regional model results, we find that RegCM4 shows, with respect to CAM3, an intensification of extreme precipitation events that we relate to the higher resolution in RegCM4 of the orography of the Mediterranean basin. Only minor differences can be found between RegCM4 and CAM3 simulations of temperature extreme events, which are probably related to the differences in the simulated heat fluxes. These results highlight the importance of regional downscaling when local climate/impact studies are performed.

Due to the nonlinearity of the high latitude circulation response to BK sea-ice wintertime decrease (Petoukhov and Semenov 2010), the discussed response is expected to be dependent on the characteristics of the prescribed sea-ice concentrations and might not be representative of a different sea-ice reduction scenarios.

Further studies, performed on simulation ensemble produced with a variety of GCMs and regional circulation models, could enable to better distinguish the response to sea-ice reduction from internal variability, then enhancing the significance of the results.

Acknowledgments.

We thank Filippo Giorgi and *ICTP* for making available the *RegCM4* model. Our thanks also go to Graziano Giuliani for assistance with model implementation and guidance with model pre- and post- processing. We thank anonymous reviewers for their valuable comments and suggestions.

References

Alexander, L. V., and Coauthors, 2006: Global observed changes in daily climate extremes of temperature and precipitation. J. Geophys. Res., 111, D05109, doi:10.1029/2005JD006290.

Arthun, M., T. Eldevik, L. H. Smedsrud, O. Skagseth and R. B. Ingvaldsen, 2012: Quantifying the Influence of Atlantic Heat on Barents Sea Ice Variability and Retreat. *J. Climate*, **25**, 4736-4743, doi:10.1175/JCLI-D-11-00466.1.

Bell, J. L., L. C. Sloan, M. A. Snyder, 2004: Regional changes in extreme climatic events. *J. Climate*, **17**(1), 81-87.

Brankovic, C., M. Patarcic, I. Guttler and L. Srnec, (2012): Near-future climate change over Europe with focus on Croatia in an ensemble of regional climate model simulations. *Clim. Res.*, **52**, 227-251, doi:10.3354/cr01058.

Collins, W. D., and Coauthors, 2006: The Formulation and Atmospheric Simulation of the Community Atmosphere Model Version 3 (CAM3). *J. Climate*, **19**, 2144-2161, doi:10.1175/JCLI3760.1.

Deser, C., A. T. Robert, and S. Peng, 2007: The Transient Atmospheric Circulation Response to North Atlantic SST and Sea Ice Anomalies. *J. Climate*, **20**, 4751-4766, doi:10.1175/JCLI4278.1.

Deser, C., T. Robert, and M. Alexander, and D. Lawrence, 2010: The Seasonal Atmospheric Response to Projected Arctic Sea Ice Loss in the Late Twenty-First Century. *J. Climate*, **23**, 334-351, doi:10.1175/2009JCLI3053.1.

Diffenbaugh, N. S., J. S. Pal, R. J. Trapp, and F. Giorgi, 2005: Fine-scale processes regulate the response of extreme events to global climate change. *PNAS*, **102**, 15774-15778.

EM-DAT, 2009: The OFDA/CRED International Disaster Database, www.emdat.net, Université catholique de Louvain, Brussels.

Gao, X., J. S. Pal, and F. Giorgi, 2006: Projected changes in mean and extremes precipitation over the Mediterranean region from a high resolution double nested RCM simulation. *Geophys. Res. Lett.*, **33**, L03706, doi:10.1029/2005GL024954.

Giorgi, F., M. R. Marinucci, G. T. Bates et al., 1993: Development of a second-generation regional climate model (RegCM2). Part II: Convective processes and assimilation of lateral boundary conditions. *Mon. Wea. Rev.*, **121**, 2814–32

Giorgi, F., and Coauthors, 2012: RegCM4: model description and preliminary tests over multiple CORDEX domains. *Clim. Rev.*, **52**(1), 7-29.

Goubanova, K., and L. Li, 2007: Extremes in temperature and precipitation around the Mediterranean basin in an ensemble of future climate scenario simulations. *Global and Planetary change*, **57**, 27-42.

Grassi, B., G. Redaelli, and G. Visconti, 2008: Tropical SST preconditioning of the SH Polar Vortex during winter 2002. *J. Climate*, **21(20),** 5295-5303, doi:10.1175/2008JCLI2136.1.

Grassi, B., G. Redaelli, P. Canziani, and G. Visconti, 2012: Effects of the PDO phase on the tropical belt width. *J. Climate,* doi:10.1175/JCLI-D-11-00244.1.

Holland, M. M., C. M. Bitz and B. Tremplay, 2006: Future abrupt reductions in the summer Arctic sea ice. *Geophys. Res. Lett.*, **33**, L23503, doi:10.1029/2006GL028024.

Honda, M., J. Inoue, and S. Yamane, 2009: Influence of low Arctic sea-ice minima on anomalously cold Eurasian winters. *Geophys. Res. Lett.*, **36**, L08707, doi:10.1029/2008GL037079.

Huntingford, C., R. G. Jones, C. Prudhomme, R. Lamb, J. H. C. Gash, and D. A. Jones, 2003: Regional climate model predictions of extreme rainfall for a changing climate. *Q. J. R. Meteorol. Soc.*, **129**, 1607-1622.

Hurrell, J. W., J. J. Hack, A. S. Phillips, J. Caron, and J. Yin, 2006: The Dynamical Simulation of the Community Atmosphere Model Version 3 (CAM3), *J. Climate*, **19**, 2162-2183.

Inoue, J., M. E. Hori, and K. Takaya, 2012: The Role of Barents Sea Ice in the Wintertime Cyclone Track and Emergence of a Warm-Arctic Cold-Siberian Anomaly, *J. Climate*, **25**, 2561-2568, doi:10.1175/JCLI-D-11-00449.1.

IPCC, 2007: Climate Change 2007: The Physical Science Basis. Contribution of Working Group I to the Fourth Assessment Report of the Intergovernmental Panel on Climate Change. *Cambridge University Press*, Cambridge, United Kingdom and New York, NY, USA, 996 pp.

Jaiser, R. et al., 2012: Impact of sea ice cover changes on the Northen Hemisphere atmospheric winter circulation, *Tellus A*, **64**, doi:10.3402/tellusa.v64i0.11595.

Joughin, I., R. B. Alley and D. Holland, 2012: Ice-Sheet Response to Oceanic Forcing, *Science*, **338**, 1172-1176.

Kern, S., L. Kaleschke, and G. Spreen, 2010: Climatology of the Nordic (Irminger, Greenland, Barents, Kara and White/Pechora) Seas ice cover based on 85 GHz satellite microwave radiometry: 1992-2008. *Tellus*, **62A**, 411-434.

Kharin, V.V., F. W. Zwiers, X. Zhang, and G. C. Hegerl, 2007: Changes in temperature and precipitation extremes in the IPCC ensemble of global coupled model simulations. *J. Climate,* **20**, 1419-1444, doi:10.1175/JCLI4066.1.

Klein Tank, A. M. G., and G. P. Konnen, 2003: Trends in indices of daily temperature and precipitation extremes in Europe, 1946-99. *J. Climate,* **16**, 3665-3680, doi:10.1175/1520-0442(2003)016<3665:TIIODT>2.0.CO;2.

Kodra, E., K. Steinhaeuser, and A. R. Ganguly, 2011: Pesisting cold extremes under 21st-century warming scenarios. *Geophys. Res. Lett.*, **38**, L08705, doi:10.1029/2011GL047103.

Liu, et al., 2012: Impact of declining Arctic sea ice on winter snowfall. *PNAS,* **109**, 4074-4079.

Meehl, G. A., C. Tebaldi, and D. Nychka, 2004: Changes in frost days in simulations of twenty-first century climate. *Clim. Dyn*., **23**, 495-511, doi:10.1007/s00382-004-0442-9.

Petoukhov, V. and V. A. Semenov, 2010: A link between reduced Barents-Kara sea ice and cold winter extremes over northern continents. *J. Geophys. Res.,* **115**, D21111, doi:10.1029/2009JD013568.

Rayner, N. A., and Coauthors, 2003: Global analyses of sea surface temperature, sea ice, and night marine air temperature since the late nineteenth century. *J. Geophys. Res.*, **108**(D14), 4407, doi:10.1029/2002JD002670.

Reynolds, R. W., and Coauthors, 2002: An improved in situ and satellite SST analysis for climate. *J. Climate,* **15**, 1609-1625.

Smith, I., A. Moise, J. Katzfey, K. Nguyen, R. Colman, 2013: Regional scale rainfall projections-simulations for the New Guinea region using the CCAM model. *J. Geophys. Res.*, accepted, doi:10.1002/jgrd.50139.

Stroeve, J., M. M. Holland, W. Meier, T. Scambos, and M. Serreze, 2007: Arctic sea ice decline: Faster than forecast. *Geophys. Res. Lett.*, **34**, L09501, doi:10.1029/2007GL029703.

Stroeve, J. and Coauthors, 2011: The Arctic's rapidly shrinking sea ice cover: a research synthesis. *Climatic Change*, doi:10.1007/s10584-011-0101-1.

Takaya, K., and N. Nakamura, 2001: A Formulation of a Phase-Independent Wave-Activity Flux for Stationary and Migratory Quasigeostrophuc Eddies on a Zonally Varying Basic Flow. *J. Atmos. Sci*., **58**, 608-627.

Toreti, A., E. Xoplaki, D. Maraun, F. G. Kuglitsch, H. Wanner, and J. Luterbacher, 2010: Characterization of extreme winter precipitation in Mediterranean coastal sites and associated anomalous atmospheric circulation patterns. *Nat. Hazards Earth Syst. Sci*., **10**, 1037-1050.

Yamamoto, K. Y. Tachibana, M. Honda, and J. Ukita, 2006: Intra-seasonal relationship between the Northen Hemisphere sea ice variability and the North Atlantic Oscillation. *Geophys. Res. Lett.*, **33**, L14711, doi:10.1029/2006GL026286.

____

B. Grassi, G. Redaelli , and G. Visconti, CETEMPS/Department of Physics, University of L'Aquila, Coppito-L'Aquila, Italy.
(e-mail barbara.grassi@aquila.infn.it)

____

GRASSI ET AL.: ARCTIC SEA-ICE AND MEDITERRANEAN CLIMATE EXTREMES

Figure 1. November to April mean of sea-ice concentration (%) boundary conditions, used in the 50%ICE (left) and 20%ICE (right) simulation cases.

Figure 2. CAM3 simulated change (20%ICE minus 50%ICE) of: (left) Surface Level Pressure (SLP), for January; (right) baroclinicity (m s^{-1} km^{-1}), for November. Green contour lines encompass anomalies that are statistically significant at 95% confidence level.

Figure 3. CAM3 simulation of: (left) change (20%ICE minus 50%ICE) of 500 hPa geopotential height; (right) 500 hPa geopotential height in the background 50%ICE case. Both plots are for January. Green contour lines encompass anomalies that are statistically significant at 95% confidence level.

Figure 4. Difference map (20%ICE minus 50%ICE), as simulated by CAM3 for winter, of

surface sensible and latent heat fluxes (W m^{-2}, positive: upward; color shaded), 250 hPa horizontal wave activity flux (m s^{-2}, arrows) and 250 hPa geopotential height (m, isolines).

Figure 5. CAM3 simulated change (20%ICE minus 50%ICE) of monthly mean daily minimum temperature (T_{min}) for January (top), February (middle) and March (bottom). Green contour lines encompass anomalies that are statistically significant at 95% confidence level.

Figure 6. Upper plots: RegCM4 (a) and CAM3 (b) simulated change (20%ICE minus 50%ICE) of sensible and latent heat flux. Bottom plots: sensible and latent heat flux, as simulated in the background 50%ICE case by RegCM (c) and CAM3 (d). Only statistically significant anomalies at the 95% confidence level are shown.

Figure 7. Difference maps (20%ICE minus 50%ICE) of: (a,d) $<T_{min}>$ (°C), (b,e) T_{min}^{05} (°C), (c,f) N_{cold} (days), as simulated by RegCM4 and CAM3, respectively (see text for index definitions). Only statistically significant anomalies at the 95% confidence level are shown.

Figure 8. Difference maps (20%ICE minus 50%ICE) of: (a,d) $<P_{tot}>$ (mm/day), (b,e) P_{tot}^{95} (mm/day), (c,f) N_{rainy} (days), as simulated by RegCM4 and CAM3, respectively (see text for index definitions). Only statistically significant anomalies at the 95% confidence level are shown.

Figure 1
Click here to download Rendered Figure: Figure_1.pdf

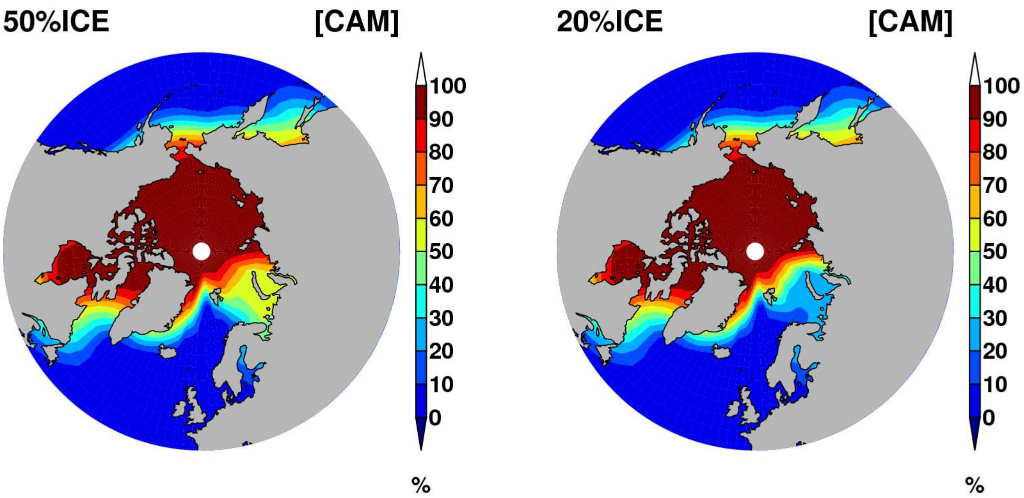

Figure 1. November to April mean of sea-ice concentration (%) boundary conditions, used in the 50%ICE (left) and 20%ICE (right) simulation cases.

Figure 2
Click here to download Rendered Figure: Figure_2.pdf

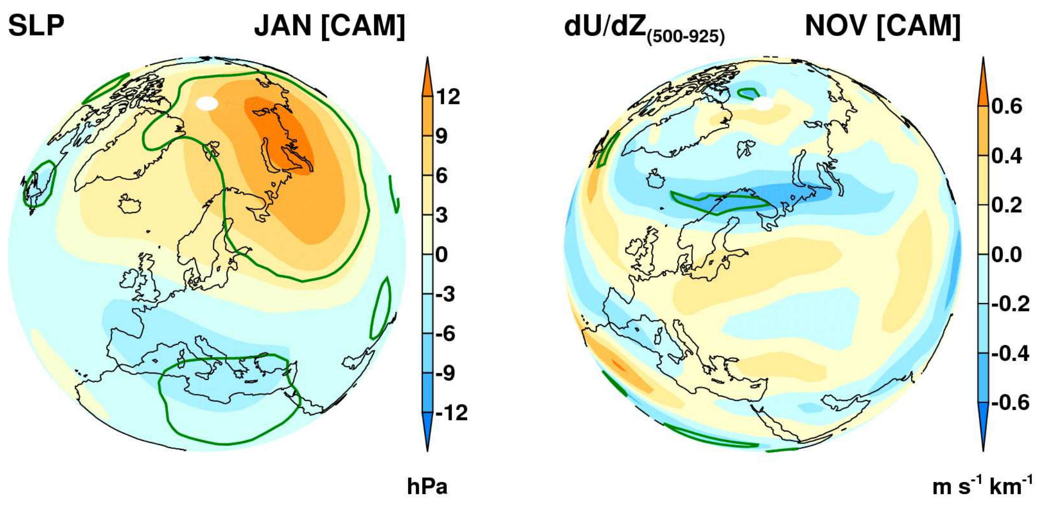

Figure 2. CAM3 simulated change (20%ICE minus 50%ICE) of: (left) Surface Level Pressure (SLP), for January; (right) baroclinicity (m s^{-1} km^{-1}), for November. Green contour lines encompass anomalies that are statistically significant at 95% confidence level.

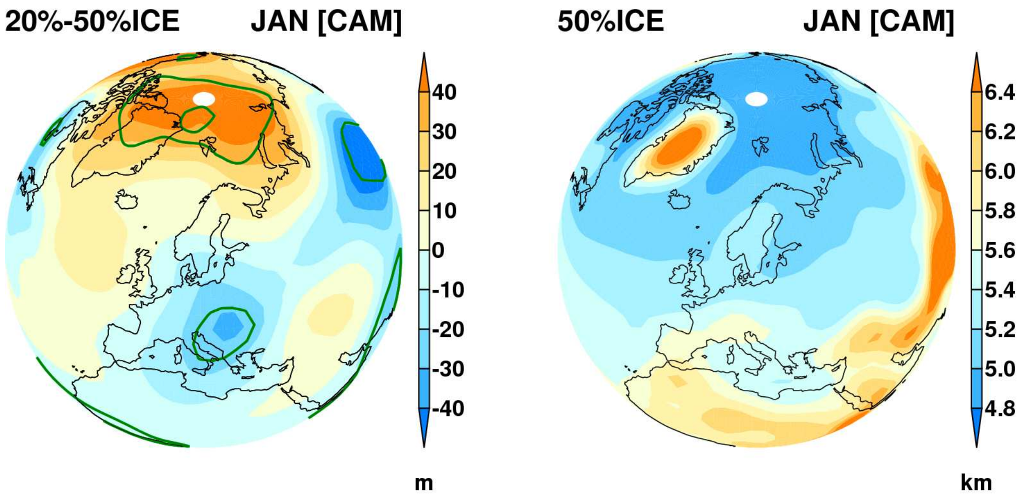

Figure 3. CAM3 simulation of: (left) change (20%ICE minus 50%ICE) of 500 hPa geopotential height; (right) 500 hPa geopotential height in the background 50%ICE case. Both plots are for January. Green contour lines encompass anomalies that are statistically significant at 95% confidence level.

Figure 4
Click here to download Rendered Figure: Figure_4.pdf

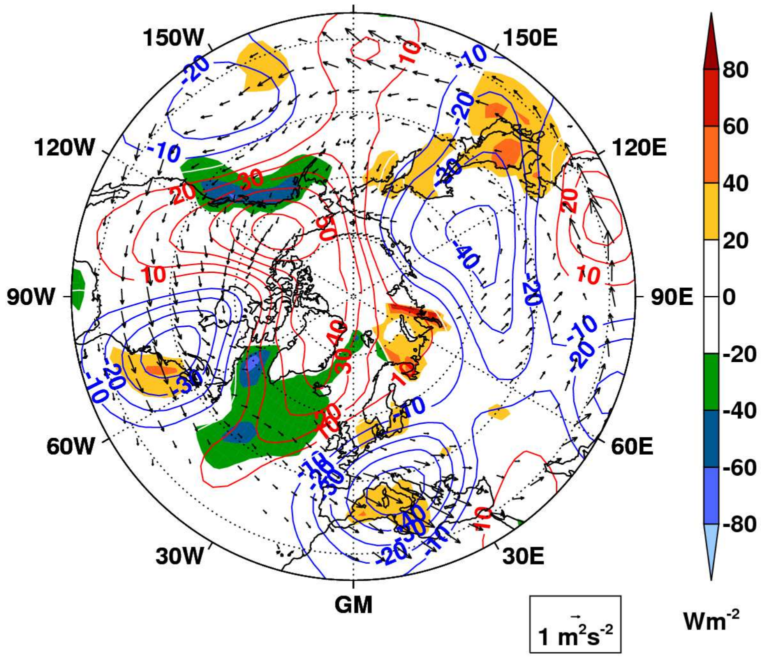

Figure 4. Difference map (20%ICE minus 50%ICE), as simulated by CAM3 for winter, of surface sensible and latent heat fluxes (W m^{-2}, positive: upward; color shaded), 250 hPa horizontal wave activity flux (m s^{-2}, arrows) and 250 hPa geopotential height (m, isolines).

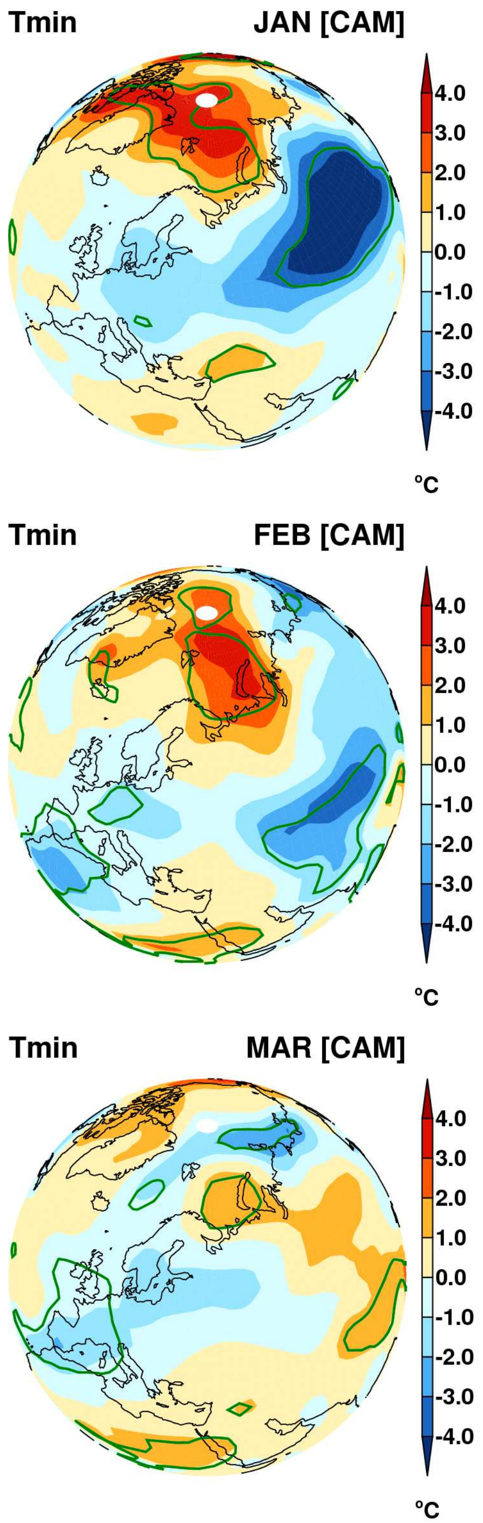

Figure 5. CAM3 simulated change (20%ICE minus 50%ICE) of monthly mean daily minimum temperature (T_{min}) for January (top), February (middle) and March (bottom). Green contour lines encompass anomalies that are statistically significant at 95% confidence level.

Figure 6
Click here to download Rendered Figure: Figure_6.pdf

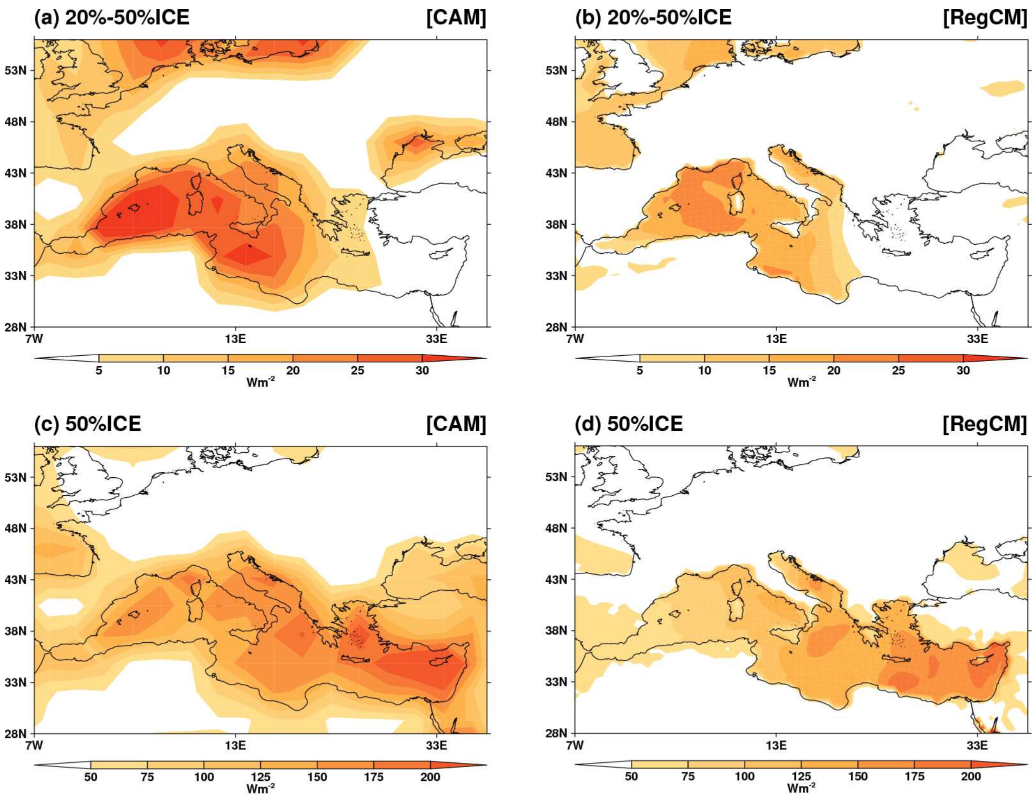

Figure 6. Upper plots: RegCM4 (a) and CAM3 (b) simulated change (20%ICE minus 50%ICE) of sensible and latent heat flux. Bottom plots: sensible and latent heat flux, as simulated in the background 50%ICE case by RegCM (c) and CAM3 (d). Only statistically significant anomalies at the 95% confidence level are shown.

Figure 7

Click here to download Rendered Figure: Figure_7.pdf

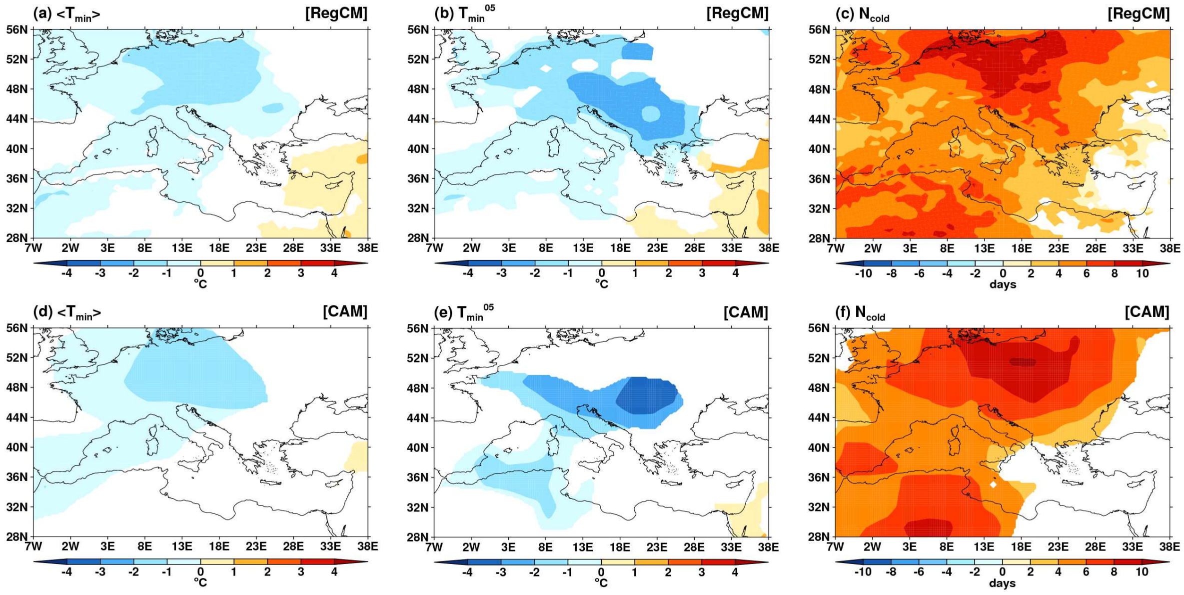

Figure 7. Difference maps (20%ICE minus 50%ICE) of: (a,d) $<T_{min}>$ (°C), (b,e) T_{min}^{05} (°C), (c,f) N_{cold} (days), as simulated by RegCM4 and CAM3, respectively (see text for index definitions). Only statistically significant anomalies at the 95% confidence level are shown.

Figure 8

Click here to download Rendered Figure: Figure_8.pdf

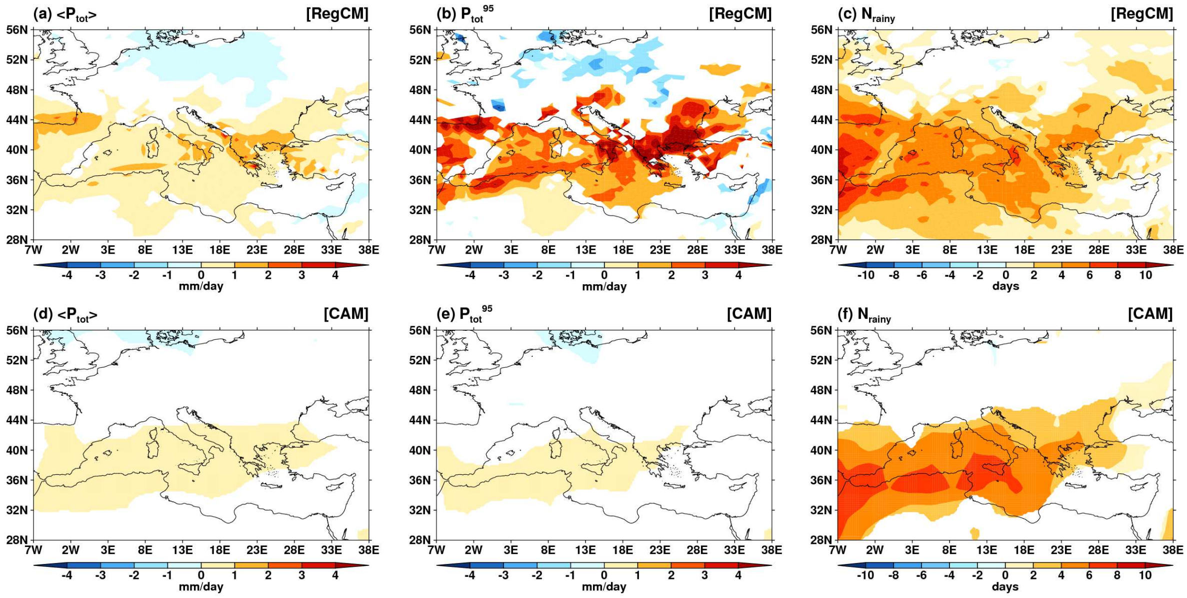

Figure 8. Difference maps (20%ICE minus 50%ICE) of: (a,d) $\langle P_{tot} \rangle$ (mm/day), (b,e) P_{tot}^{95} (mm/day), (c,f) N_{rainy} (days), as simulated by RegCM4 and CAM3, respectively (see text for index definitions). Only statistically significant anomalies at the 95% confidence level are shown.